Test of KW Class Photonic Microwave Generation Using Vanadium-Compensated 6H-SiC PCSS and Burst-Mode-Operation Pulse Laser

Xinyue Niu, Qilin Wu, Bin Wang, Jinmei Yao, Xu Chu, Muyu Yi, Yanran Gu, Langning Wang, Tao Xun, and Hanwu Yang

***Abstract*—Photoconductive semiconductors operating in linear mode can be used for adaptive high-power microwave (HPM) generators by modulating incident light. This paper presents the design scheme and preliminary test results of a narrowband kW class adaptive photonic microwave generator by employing a wide-bandgap semi-insulating 6H-SiC photoconductive semiconductor and a burst-mode laser. The experimental scheme of the generator is described along with the circuit simulation of the radio frequency generator. The laser operated at a wavelength of 532 nm with a pulse width of 100 ns and a repetition rate of 100 Hz. The laser modulates the frequencies of the generated microwave, and preliminary tests are conducted in the frequency range of 0.8–1.2 GHz. The maximum output microwave power of the designed scheme reaches up to 2.6 kW when the bias voltage is 10 kV. The results confirm that this method can be used for high-power frequency-adjustable microwave signal generation. The microwave source system presented in this paper has continuously adjustable frequency and flexible waveform control.**

***Index Terms*—Burst-mode-operation pulse laser, frequency-adjustable high power microwave generation, photoconductive semiconductor device.**

I. Introduction

HIGH-power microwave sources have been widely studied due to their potential applications in pulse radar and continuous wave radar [3], radio frequency (RF) acceleration of charged particles, microwave sources for plasma heating [4], and directed-energy systems [5], [6]. The demand for these applications promotes the development of microwave sources.

Vacuum electronic devices are frequently used as narrowband high-power microwave (HPM) generators with GW-level output power. However, microwaves generated by traditional relativistic electron devices generally operate with fixed output parameters, making it difficult to change the frequency rapidly and continuously [7], [8]. Besides, the size of the vacuum tube is bulky in general. In recent years, with the rapid development of the third generation of semiconductors such as GaN, the peak power of solid-state electric amplifiers has been continuously improved, making it possible to generate HPMs [9], [10]. However, the single device power is limited to kW or several kW [11].

The scheme of high-power microwave photonics has several advantages compared to the conventional electric power amplifier, e.g., increasing efficiency by eliminating the electric polarity, reducing the system complexity by omitting the input matching network and gating bias circuitry, and improving the output power by stacking photoconductive semiconductors illuminated in isolation.

One of the microwave photonics methods is based on photoconductive semiconductor switches (PCSS). PCSSs have linear and nonlinear operation modes, and their working mechanisms differ. A nonlinear PCSS device is switched on by a laser with lower optical excitation energy of nJ level. A small number of carriers are generated in the semiconductor and amplified by a field-avalanche mechanism called 'lock-on'. Current remains after laser pulses trigger PCSS and decays with the attenuation of the electric field. The PCSS operating in nonlinear mode can deliver the unipolar or bipolar high voltage pulses to the load or antenna. The time domain response of nonlinear photoconductive devices is an impulse pulse with pulse widths of a few ns and rise and fall times of hundreds of picoseconds, which determines its central frequency (usually <1 GHz) and makes it difficult to control the flexible change of waveform [12].

The photoconductive semiconductors operating in linear mode exhibit light-controlled resistance. Thus, it is possible to generate adaptive high-power RF or microwave fields. A photoconductive semiconductor with a linear operating mode is more stable than a nonlinear operating mode, with less jitter between the output electrical pulse and the trigger light pulse [13]. Therefore, the narrowband microwave produced in this manner is easier to synthesize than the wide-band or ultra-wide-band microwave produced by the photoconductive semiconductor operating in a nonlinear mode. The responsive current generated in PCSS operating in linear mode is more uniform, which benefits its long-life operation.

Manuscript received 29 August 2022; accepted 8 September 2022. Date of publication 13 September 2022; date of current version 3 February 2023. This work was supported in part by the National Natural Science Foundation of China under Grant 62071477, in part by the National Natural Science Foundation of China under Grant 62101577, and in part by the Natural Science Foundation of Hunan Province under Grant 2021JJ40660. *(Xinyue Niu and Qilin Wu contributed equally to this work.) (Corresponding authors: Tao Xun; Jinmei Yao.)*

The authors are with the College of Advanced Interdisciplinary Studies, National University of Defense Technology, Changsha 410073, China (e-mail: xinyuee.niu@outlook.com; kylinwu570@163.com; 3431471977@qq.com; yaojinmei@nudt.edu.cn; 15580957460@163.com; 461670546@qq.com; 584217552@qq.com; wanglangning@126.com; xtao_0301@hotmail.com; yanghw@nudt.edu.cn).

Digital Object Identifier 10.1109/JPHOT.2022.3206209

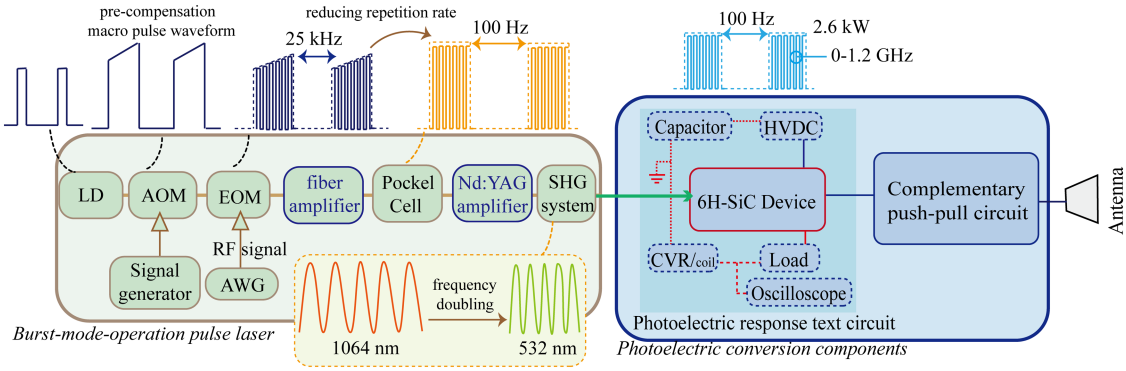

Fig. 1. The designed scheme of the frequency-adjustable HPM generator based on a linear 6H-SiC PCSS, including the photoelectric conversion components and the burst-mode-operation pulse laser [33].

The wide-bandgap materials have a higher breakdown field (>2 MV/m), higher saturated electron velocity (2×10^7 cm/s), and higher thermal conductivity (3–5 W/cm·K) [14], [15], [16], [17], [18], [19], [20]. These advantages make wide-bandgap materials a better choice in high-voltage and high-temperature environments. Wu et al. [30], [31], [32], have proved that 6H-SiC photoconductive semiconductors can produce photocurrents that change linearly with applied voltage and optical energy. They have also proposed that this method could be used for microwave generators in 2019 [21].

In this paper, a narrowband high-power frequency-adjustable RF/microwave generation scheme was proposed and demonstrated based on a linear mode vanadium-compensated 6H-SiC photoconductive device and a high-energy burst-mode fiber laser. Section II introduces the device structure and the components of the experiment. In Section III, a simulation model of the 6H-SiC device is built to predict and analyze the system performance. Next, Section IV shows experimental results of various modulated laser frequencies and analyzes them. Section V contains the summary, the improvement direction, and the development potential of the systems.

II. Experimental Setup

A. Components of the Experiment

Fig. 1 shows the experimental setup, including the burst-mode laser and the 6H-SiC device. The burst-mode laser has the characteristics of continuously adjustable intra-burst repetition rate and high peak power. Generally, it can be used for material processing in industrial and surgery areas [24], [25]. Also, it can be used for generating radio-frequency waves when combined with semiconductor materials [26], [27], [28], [29]. The setup of the burst-mode laser is similar to the structure described in [33]. The repetition and duration of the electrical pulse-driven narrowband LD are set as 25 kHz and 100 ns, respectively. The acousto-optic modulator (AOM) with a high extinction ratio is employed to program the temporal pulse waveform to compensate for the envelope distortion induced by the gain saturation effect. The distorted temporal profile of the amplified burst-mode laser is high in the front and low in the back. Moreover, the AOM is programmed with the calculated transfer function so that the signal passing through it is low in the front and high in the back. Thus, a pre-compensation technique is adopted to realize the homogenous energy distribution in each burst by the AOM.

Then, an electro-optical modulator (EOM) accompanied by an arbitrary waveform generator (AWG) modulates the laser pulse into burst-mode operation with modulating frequency. Thus, a burst-mode seed laser with milliwatt-level average power is obtained by combining AOM and EOM. After that, the seed laser is amplified by a three-stage all-fiber amplifier. Thus, the output optical peak power can reach 8 kW. Then the Pockel Cell is utilized to reduce the burst repetition rate from 25 kHz to 100 Hz. A two-stage solid-state amplifier further amplifies the laser. Next, the 1064 nm laser is changed to a 532 nm laser by a secondary harmonic generation (SHG) system. The diameter of the light spot after an optical beam expander is 6 mm, and the beam directly passes through the hollow copper electrode onto the 6H-SiC device.

During the experiment, the bias voltage of the 6H-SiC device varies from 1 kV to 10 kV. As for the circuit, a 100 Ω load resistor is in series with the 6H-SiC device, while a capacitor is discharged through them. The output photocurrent is detected by a current viewing resistor (CVR) with a resistance of 0.1 Ω and a rise-time of 180 ps. The load voltage is measured using a Northstar model PVM-1 high voltage probe. An Agilent oscilloscope with a bandwidth of 32 GHz and a sampling rate of 80 GS/s is used for data acquisition.

B. 6H-SiC Device Structure

With the use of vanadium-compensated semi-insulating (VCSI), 6H-SiC owns high dark resistivity ($\sim 10^{12}$ Ω· cm) and can be triggered by a laser with a wavelength below its bandgap (3 eV) [22], [23]. The wafer is sliced from the a-plane of a VCSI 6H-SiC crystal to obtain a micropipe-free substrate having dimensions 1 cm × 1 cm × 1 mm. The vertical geometry structure of the 6H-SiC device is shown in Fig. 2(a), where the laser can pass through the hollow cathode. The laser illuminates the 6H-SiC device from the contact face rather than the narrow side facets because the contact face is larger, and it is easier to control the laser illumination. The upper surface of SiC is coated with a transparent electrode, Al-doped ZnO (AZO), to

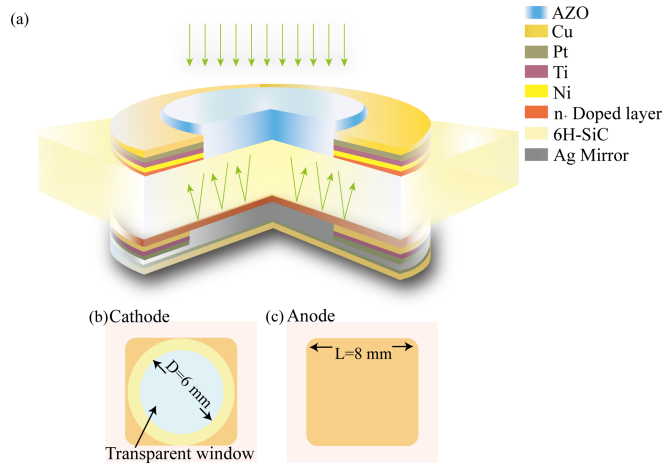

Fig. 2. The 6H-SiC device structure. (a) Profile of the V-doped 6H-SiC device, (b) Cathode of the device, (c) Anode of the device.

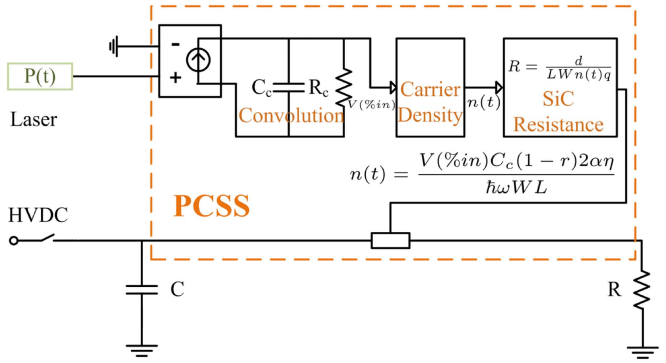

Fig. 3. The circuit model of the radio-frequency generating system in PSpice.

TABLE I
THE PARAMETERS OF THE SELECTED 6H-SIC

Properties	Symbol	Value	units
Quantum efficiency	η	0.1	-
Reflection coefficient	r	0.2	-
Absorption coefficient	α	0.8	cm^{-1}
Recombination time	τ_r	0.13×10^{-9}	s
Length	L	11×10^{-1}	cm
Width	w	11×10^{-1}	cm
Thickness	d	200	μm
Electron mobility	μ_e	0.1	$cm^2/(Vs)$

increase light absorption and reduce reflection loss. The opposite surface is coated with a silver mirror reflector to enhance reflection and increase the absorption of laser light by a factor of two. The electrode-semiconductor contacts consist of a 6-mm diameter circular metallization centered on opposite sides of the substrate. Cylindrical copper electrodes are glued with silver to the substrate metallization to facilitate electrical connections. The cathode and anode are shown in Fig. 2(b) and (c). Epoxy has been used to fill the photoconductive semiconductor device as it has a relatively high dielectric constant and thus increases the device's breakdown voltage.

III. Simulation Model of Resistance

A circuit model of the 6H-SiC device is built to analyze the system's performance in PSpice based on the equivalent resistance formula of the photoconductive semiconductor device. Assuming constant mobility, one can easily derive the resistance of the device as a function of the input light intensity. The carrier concentration $n(t)$ is shown in (1):

$$\mathrm{n}(t) = \int_{-\infty}^{t} G(s) e^{\frac{s-t}{\tau_r}} ds \tag{1}$$

where G is the optical generation rate, and τ_r is the recombination time. The carrier concentration is produced by the convolution of the electron generation rate and the exponential decay of the recombination time. The absorption coefficient, α, is relatively small. Because of the highly reflective silver on the opposite electrode, the laser passes through the PCSS wafer twice. Thus, the electron generation rate $G(t)$ of the linear semiconductor material is given by (2):

$$G(t) = \frac{P(t)\eta(1-r)(1-e^{-2\alpha d})}{\hbar\omega W d L} \tag{2}$$

where $P(t)$ is the instantaneous input optical power, η is the quantum efficiency (the ratio of optically generated carriers to photons arriving at the substrate facet) of the semiconductor material, r is the surface reflectance of the device, d is the thickness of the semiconductor wafer, $A = 1\ \mathrm{cm}^2$ is the cross-Section of the light path, $\hbar$ is Planck constant, and ω is the laser frequency. Substituting $G(t)$ into (1), $n(t)$ can be written as:

$$\begin{aligned} n(t) &= \frac{\eta(1-r)(1-e^{-2\alpha d}) \int_{-\infty}^{t} P(s) e^{\frac{s-t}{\tau_r}} ds}{\hbar\omega W d L} \\ &= \frac{\eta(1-r)(1-e^{-2\alpha d}) e^{-\frac{t}{\tau_r}} \int_{-\infty}^{t} P(s) e^{\frac{s}{\tau_r}} ds}{\hbar\omega W d L} \end{aligned} \tag{3}$$

With the conductance $\sigma = qn\mu$, the dynamic resistance of the photoconductive semiconductor, in this case, can be written as

$$\begin{aligned} n(t) &= \frac{1}{\sigma}\frac{d}{WL} = \frac{\hbar\omega d^2}{q\mu\eta(1-r)(1-e^{-2\alpha d}) e^{-\frac{t}{\tau_r}} \int_{-\infty}^{t} P(s) e^{\frac{s}{\tau_r}} ds} \\ &\approx \frac{1}{2}\frac{\hbar\omega d}{q\mu\eta(1-r)\alpha e^{-\frac{t}{\tau_r}} \int_{-\infty}^{t} P(s) e^{\frac{s}{\tau_r}} ds} \end{aligned} \tag{4}$$

The last approximation of Eq. (4) is obtained assuming $2ad << 1$. Based on (3) and (4), a resistance model of the 6H-SiC device in PSpice can be built, as shown in Fig. 3. Important parameters of the employed 6H-SiC material are listed in Table I.

We use the resistance model in Fig. 3 to simulate the process of burst-mode laser with different frequencies illuminating the 6H-SiC device and obtaining the output current. Fig. 4 presents the simulation waveforms of the laser and the response current at modulated frequencies of 0.1 GHz, 0.5 GHz, 1.2 GHz, and

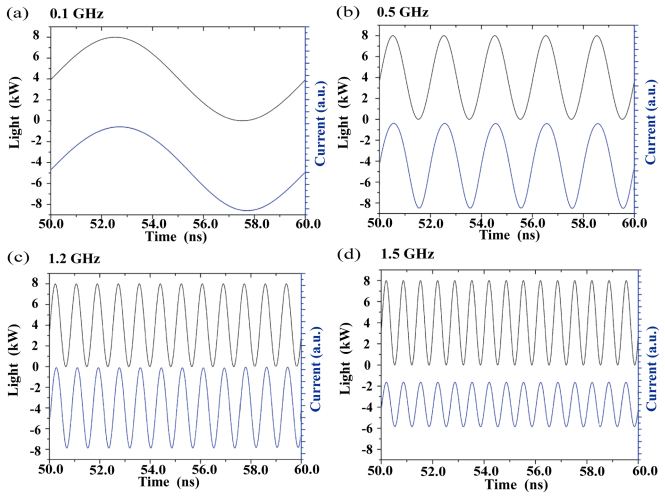

Fig. 4. The simulation waveforms of the laser and the response current at modulated frequencies of (a) 0.1 GHz, (b) 0.5 GHz, (c) 1.2 GHz, and (d) 1.5 GHz.

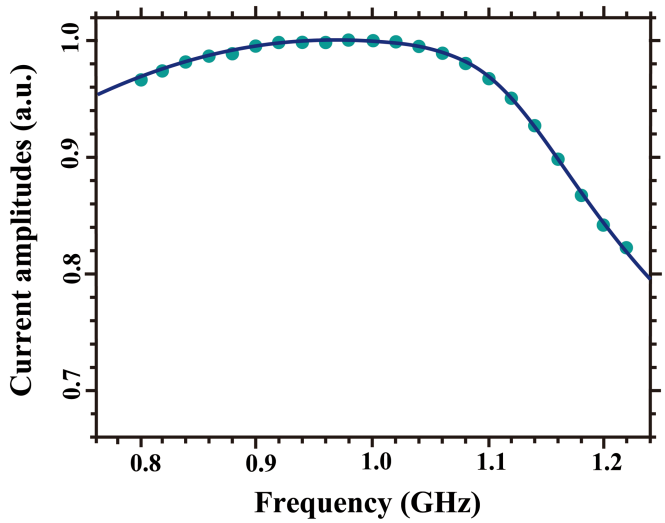

Fig. 5. The relationship between amplitude and frequency of output current in simulation results.

1.5 GHz, respectively. The upper black curves show the simulation optical waveforms. The underneath blue curves show the simulation waveforms of the output current. Results prove that the 6H-SiC device responds well to the laser with a continuously adjustable pulse repetition frequency of 0–1.5 GHz.

The PCSS has a fast response indicating short carrier recombination times. (The carrier recombination time was calculated using the method proposed by Mr. Sullivan in [14], and the result was about 150 ps.) The response time of the device is determined only by the carrier lifetime. A PCSS with a shorter carrier lifetime could be developed, enhancing the system's response to incoming light and preventing waveform distortion at higher frequencies. Assuming the carrier lifetime as the limiting factor, reducing the carrier lifetime by a factor of 10 will increase the upper response frequency limit by approximately 10.

For the device, the carrier recombination time determines the upper limit of the response frequency. In addition, the high voltage test circuit in which the device is located also impacts the response frequency. So the device response is not only limited by the carrier lifetime, but also limited by the time constant of the test circuit. The simulation results show the relationship between amplitude and frequency of output current, and the RF signal in Fig. 5 is attenuated by 3 dB at 1.44 GHz.

IV. Experiment Result and Discussion

A. Results With 532 nm Burst-Mode Laser

The VCSI 6H-SiC is excited by light with the wavelength of 532 nm, corresponding to 2.34 eV, which is lower than the bandgap of SiC (3 eV), so extrinsic absorption occurs. A pulsed laser operating at a wavelength of 532 nm is used to test the output waveforms of the PCSS.

The pulsed laser has a repetition rate of 100 Hz and a pulse width of 100 ns. The output energy of the SHG system is 1.65 mJ with the average power of 0.165 W, corresponding to a peak power density of 1.17 kW/mm^2. The normalized waveforms of input light signals are shown in Fig. 6(a), the normalized

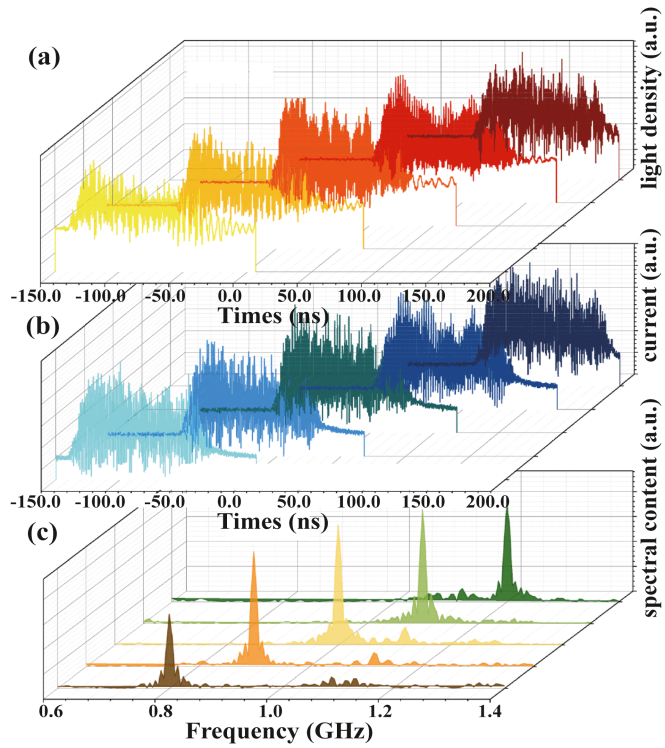

Fig. 6. The experimental result of output waveforms of the 6H-SiC device with the 532 nm pulse laser. (a) Waveforms of input light signals, (b) Current waveforms, and (c) RF spectrums.

output currents with different modulated frequencies are shown in Fig. 6(b), and the corresponding normalized RF spectrums of the output signal are shown in Fig. 6(c). It can be seen that the SiC photoconductive system can respond to a wide range of frequencies and produce modulated RF/microwave output signals.

From 0.8 to 1.2 GHz modulated frequency, the forms of the photocurrents are identical to that of the pulsed lasers, and the

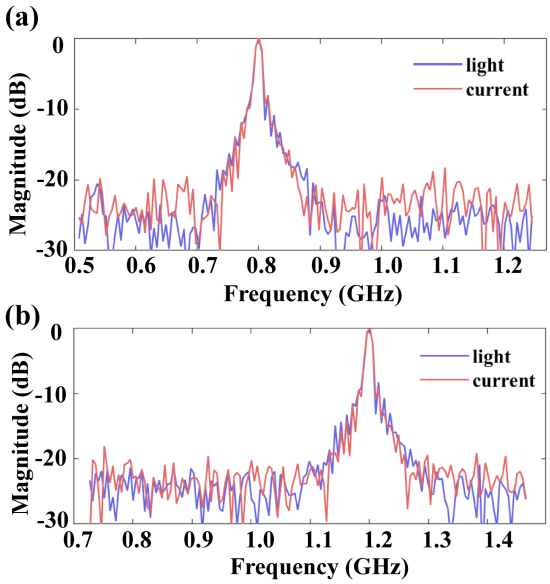

Fig. 7. Comparison of the spectrum of the original optical signal and the generated electrical signal at modulation frequencies of (a) 0.8 GHz and (b) 1.2 GHz.

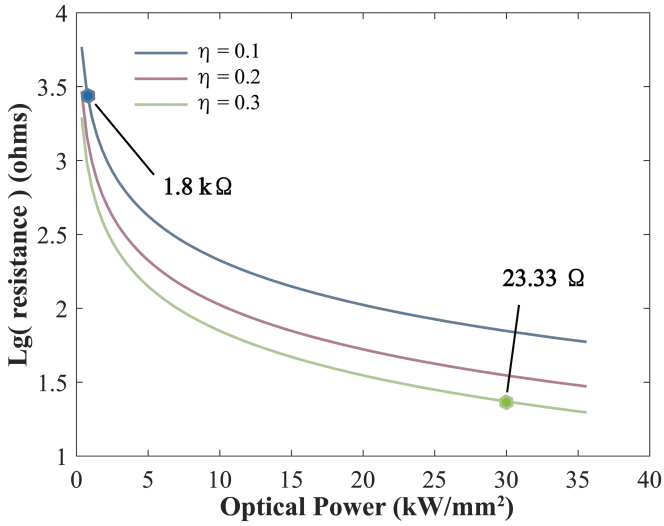

Fig. 8. The simulation result of resistance of the 6H-SiC device when illuminated with a 532 nm laser with a peak power density ranging from 0 to 35 kW/mm^2, where the quantum efficiency ranged from 0.1 to 0.3.

TABLE II
THE RESULTS OF THE EXPERIMENT

Laser wavelength (nm)	532
Laser modulated frequency (GHz)	0.8-1.2
Laser average power (W)	0.165
Laser repetition frequency (Hz)	100
Applied voltage (kV)	10
Output current (A)	5.1
Output power (kW)	2.6

output signals are narrow-spectrum signals, indicating that the VCSI 6H-SiC device indeed has a fast and linear response. The microwave generator is frequency-adjustable at around 1 GHz, verifying that the lifetime of the carriers is much less than 1 ns. The maximum output photocurrent obtained is 5.1 A, implying that the system can generate electrical power in the order of kilowatts. Hundreds of repeated experiments are conducted, and the directional coupler is used to measure the output RF signal. The frequency jitter range is less than 1%, and the amplitude jitter range is less than 3%. Furthermore, a more stable optical signal will produce a far more stable electrical signal.

In order to better observe the repetition rate of the generated electrical signal and the original optical signal, the zoomed-in spectra are shown in Fig. 7.

All the experimental data are summarized and listed in Table II.

B. Discussion of the Results

The packaged 6H-SiC device is tested in a frequency range of 0.8 GHz to 1.2 GHz, and the test results show that the photocurrent has a linear response to the incident laser. The response frequency can be further improved by optimizing the doping mechanism of VCSI 6H-SiC and reducing carrier lifetime. The RF output power is 2.6 kW when the bias voltage is 10 kV and illuminated with a 532 nm laser with an average power of 0.165 W. Combined with the simulation model; it can be seen that the main factors affecting the output power are quantum efficiency, laser power density, optical absorption efficiency, and applied voltage.

A high quantum efficiency will improve the photo-generated carrier density, thus reducing the conducting resistance. Factors affecting the efficiency η in (4) are the material properties of V-doped 6H-SiC, such as the doping concentration of Vanadium and Nitrogen.

If the two-stage solid-state amplifier does not amplify the laser pulse, the output power density of the fiber amplifier is only 0.28 kW/mm^2. At this illumination level, the on-resistance of PCSS is high, resulting in a small photocurrent. This is consistent with the conclusion that the conducting resistance is inversely proportional to the power of the input laser. By analysis, the resistance of the 6H-SiC device is approximately 1.8 kΩ at the optical peak power density of 1.17 kW/mm^2 and decreases to 23.33 Ω when the laser power density increases to 30 kW/mm^2, as shown in Fig. 8, where the load resistance is assumed to be 50 Ω and the applied voltage is assumed to be 30 kV.

As illustrated in Fig. 9, improving optical power and quantum efficiency is an important method to reduce the minimum resistance of 6H-SiC, which can significantly improve the output power of the 6H-SiC devices. The output power obtained by simulation is 8.37 MW when the laser power increases to 30 kW/mm^2, and the quantum efficiency increases to 0.3.

In Section II-B, the silver layer increases the optical path and doubles the laser absorption, showing that the device structure directly affects the optical absorption efficiency. The corresponding absorption depth of 532 nm laser in SiC substrate varies from 5 mm to 10 mm, whereas the typical thickness of

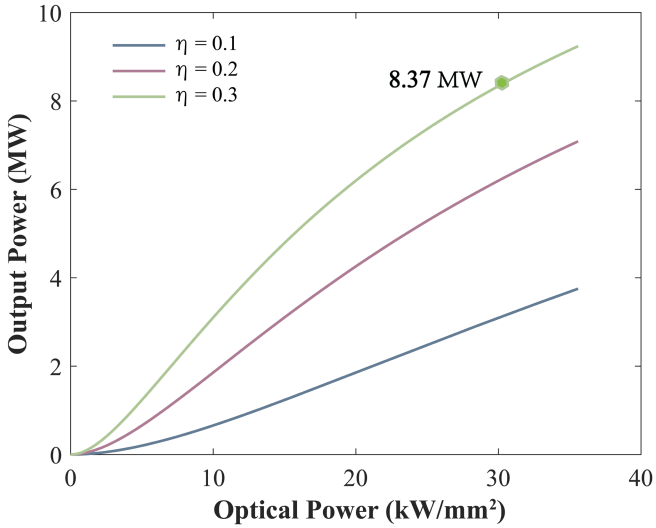

Fig. 9. The simulation result of the output power of the 6H-SiC device when illuminated with a 532 nm laser with a peak power density ranging from 0 to 35 kW/mm^2, where the quantum efficiency ranged from 0.1 to 0.3.

SiC substrate is 1 mm. Thus, optimizing the optical coupling structure can be significant future work. At last, a package structure with a high dielectric constant is used to increase the breakdown voltage and improve the device's power capacity and output voltage.

The amplitude flatness of the input light signals and the generated current waveforms are not satisfactory due to the noise caused by the introduction of Pockel Cell, a two-stage solid-state amplifier, and secondary harmonic generation (SHG) system. In the subsequent experiments, it is hoped to reduce the introduced noise and optimize the waveform by selecting an appropriate scheme. For example, using the AOM pre-compensation method, this part's influence on waveform distortion can be reduced.

V. Conclusion

The circuit simulation and experimental results show that the proposed scheme based on a VCSI 6H-SiC device and high-energy burst-mode laser has the potential to become a narrowband frequency-adjustable high-power RF/microwave generator. Due to its low jitter and ability to generate frequency-adjustable RF output signals, this scheme enables the power synthesis of many devices for increased output power. The system has the potential to become a compact microwave source, thus this scheme has the ability to satisfy more mobile applications in the HPM system.

The power capacity depends on the breakdown field of the 6H-SiC device and the power density of the laser. The device is not damaged under current light energy and voltage conditions. It can be predicted that the output RF power can be further improved by increasing the quantum efficiency, light intensity and applied voltage. According to the kilowatt-level verification experiments and the simulation results, it can be expected that when optical peak power density increases to 30 kW/mm^2, the output power of the 6H-SiC device will reach several MW.

In the future, the authors intend to use multiple SiC devices in parallel to synthesize the microwave signals for obtaining a GW microwave generator.

Data Availability

The data that supports the findings of this study is available from the corresponding author upon reasonable request.

Acknowledgment

The authors would like to express their gratitude to EditSprings (https://www.editsprings.cn) for the expert linguistic services provided.

References

[1] A. J. Seeds and K. J. Williams, "Microwave photonics," *J. Lightw. Technol.*, vol. 24, no. 12, pp. 4628–4641, Dec. 2006.
[2] J. Capmany and D. Novak, "Microwave photonics combines two worlds," *Nature Photon.*, vol. 1, no. 6, pp. 319–330, 2007.
[3] J. Yao, "Arbitrary waveform generation," *Nature Photon.*, vol. 4, no. 2, pp. 79–80, 2010.
[4] T. D. Borisova, N. F. Blagoveshchenskaya, A. S. Kalishin, M. T. Rietveld, T. K. Yeoman, and I. Hgstrm, "Modification of the high-latitude ionospheric F region by high-power HF radio waves at frequencies near the fifth and sixth electron gyroharmonics," *Radiophys. Quantum Electron.,* vol. 58, no. 8, pp. 561–585, 2016.
[5] D. Adamy, *Introduction to Electronic Warfare Modeling and Simulation*. Raleigh, NC, USA: SciTech Publishing, 2006.
[6] D. Marpaung, C. Roeloffzen, R. Heideman, A. Leinse, S. Sales, and J. Capmany, "Integrated microwave photonics," *Laser Photon. Rev.*, vol. 7, no. 4, pp. 506–538, 2013.
[7] B. L. Beaudoin et al., "Highly efficient, megawatt-class, radio frequency source for mobile ionospheric heaters," *J. Electromagn. Wave Appl.*, vol. 31, no. 17, pp. 1786–1801, 2017.
[8] J. Zhang et al., "Research progresses on Cherenkov and transit-time high-power microwave sources at NUDT," *Matter Radiat. Extremes*, vol. 1, no. 3, pp. 163–178, 2016.
[9] J. D. McKinney, "Photonics illuminates the future of radar," *Nature*, vol. 507, no. 7492, pp. 310–312, 2014.
[10] J. Benford, J. A. Swegle, and E. Schamiloglu, *High Power Microwaves,* 3rd ed. Boca Raton, FL, USA: CRC Press, 2015.
[11] R. M. O'Connell, C. -J. Huang, A. Karabegovic, and W. C. Nunnally, "Optoelectronic microwave power amplifiers," *IEEE Trans. Dielectrics Elect. Insul.,* vol. 14, no. 4, pp. 994–1001, Aug. 2007.
[12] O. S. F. Zucker, P. K.-L. Yu, and A. Griffin, "Photoconductive switch-based HPM for airborne counter-IED applications," *IEEE Trans. Plasma Sci.*, vol. 42, no. 5, pp. 1285–1294, May 2014.
[13] W. Wang et al., "Research on synchronization of 15 parallel high gain photoconductive semiconductor switches triggered by high power pulse laser diodes," *Appl. Phys. Lett.*, vol. 106, no. 2, 2015, Art. no. 022108.
[14] J. S. Sullivan, "Wide bandgap extrinsic photoconductive switches," Ph.D. dissertation, Lawrence Livermore Nat. Lab., Univ. California, Livermore, CA, USA, 2013.
[15] C. Ma, L. Yang, S. Wang, Y. Ji, L. Zhang, and W. Shi, "Study of the lifetime of high-power GaAs PCSSs under different energy storage modes," *IEEE Trans. Power Electron.*, vol. 32, no. 6, pp. 4644–4651, Jun. 2017.
[16] R. M. O'Connell, C.-J. Huang, A. Karabegovic, and W. C. Nunnally, "Optoelectronic microwave power amplifiers," *IEEE Trans. Dielectrics Elect. Insul.,* vol. 14, no. 4, pp. 994–1001, Aug. 2007.
[17] A. Karabegovic, R. M. O'Connell, and W. C. Nunnally, "Photoconductive switch design for microwave applications," *IEEE Trans. Dielectrics Elect. Insul.*, vol. 16, no. 4. pp. 1011–1019, Aug. 2009.
[18] J. Y. Tsao et al., "Ultrawide-bandgap semiconductors: Research opportunities and challenges," *Adv. Electron. Mater.*, vol. 4, no. 1, 2018, Art. no. 1600501.
[19] C. M. Zettering, *Process Technology for Silicon Carbide Devices*. London, U.K.: Institution of Engineering and Technology, 2002.

[20] D. Mauch, W. Sullivan, A. Bullick, A. Neuber, and J. Dickens, "High power lateral silicon carbide photoconductive semiconductor switches and investigation of degradation mechanisms," *IEEE Trans. Plasma Sci.*, vol. 43, no. 6, pp. 2021–2031, Jun. 2015.

[21] Q. Wu, T. Xun, Y. Zhao, H. Yang, and W. Huang, "The test of a high-power, semi-insulating, linear-mode, vertical 6H-SiC PCSS," *IEEE Trans. Electron Devices*, vol. 66, no. 4, pp. 1837–1842, Apr. 2019.

[22] P. Cao, W. Huang, H. Guo, and Y. Zhang, "Performance of a vertical 4H-SiC photoconductive switch with AZO transparent conductive window and silver mirror reflector," *IEEE Trans. Electron Devices*, vol. 65, no. 5, pp. 2047–2051, May 2018.

[23] M. E. Levinshtein, S. L. Rumyantsev, and M. S. Shur, *Properties of Advanced Semiconductor Materials: GaN, AlN, InN, BN, SiC, SiGe*. Hoboken, NJ, USA: Wiley, 2001.

[24] C. Kerse et al., "Ablation-cooled material removal with ultrafast bursts of pulses," *Nature*, vol. 537, no. 7618, pp. 84–88, 2016.

[25] S. H. Chung and E. Mazur, "Surgical applications of femtosecond lasers," *J. Biophoton.*, vol. 2, no. 10, pp. 557–572, 2010.

[26] A. Karabegovic, R. M. O'Connell, and W.C. Nunnally, "Photoconductive switch design for microwave applications," *IEEE Trans. Dielectrics Elect. Insul.,* vol. 16, no. 4, pp. 1011–1019, Aug. 2009.

[27] H. Kalaycıoğlu et al., "1 mJ pulse bursts from a Yb-doped fiber amplifier," *Opt. Lett.*, vol. 37, no. 13, pp. 2586–2588, 2012.

[28] M. Nie, X. Cao, Q. Liu, E. Ji, and X. Fu, "100 μJ pulse energy in burst-mode-operated hybrid fiber-bulk amplifier system with envelope shaping," *Opt. Exp.,* vol. 25, no. 12, pp. 13557–13566, 2017.

[29] T. Chen, H. Liu, W. Kong, and R. Shu, "Burst-mode-operated, sub-nanosecond fiber MOPA system incorporating direct seed-packet shaping," *Opt. Exp.,* vol. 24, no. 18, pp. 20963–20972, 2016.

[30] Q. Wu, Y. Zhao, T. Xun, H. Yang, and W. Huang, "Initial test of opto-electronic high power microwave generation from 6H-SiC photoconductive switch," *IEEE Electron Device Lett.*, vol. 40, no. 7, pp. 1167–1170, Jul. 2019.

[31] X. Chu et al., "Wide-range frequency-agile microwave generation up to 10 GHz based on vanadium-compensated 4H-SiC photoconductive semiconductor switch," *IEEE Electron Device Lett.*, vol. 43, no. 7, pp. 1013–1016, Jul. 2022, doi: 10.1109/LED.2022.3179292.

[32] X. Chu et al., "MHz repetition frequency, hundreds kilowatt, and sub-nanosecond agile pulse generation based on linear 4H-SiC photoconductive semiconductor," *IEEE Trans. Electron Devices*, vol. 69, no. 2, pp. 597–603, Feb. 2022, doi: 10.1109/TED.2021.3138950.

[33] X. He, B. Zhang, C. Guo, L. Yang, and J. Hou, "4 mJ rectangular- envelope GHz-adjustable burst-mode fiber-bulk hybrid laser and second-harmonic generation," *IEEE Photon. J.,* vol. 13, no. 1, Feb. 2021, Art no. 1501009, doi: 10.1109/JPHOT.2020.3048997.